Inertial Confinement Fusion Reactors Based on the Gas Protection Concept

S.I. Abdel-Khalik, G.A. Moses, and R.R. Peterson

January 1980

UWFDM-341

FUSION TECHNOLOGY INSTITUTE

UNIVERSITY OF WISCONSIN

MADISON WISCONSIN

Inertial Confinement Fusion Reactors Based on the Gas Protection Concept

S.I. Abdel-Khalik, G.A. Moses, and R.R. Peterson

Fusion Technology Institute
University of Wisconsin
1500 Engineering Drive
Madison, WI 53706

http://fti.neep.wisc.edu

January 1980

UWFDM-341

INERTIAL CONFINEMENT FUSION REACTORS

BASED ON THE GAS PROTECTION CONCEPT

S.I. Abdel-Khalik, G.A. Moses, and R.R. Peterson

Nuclear Engineering Department and Fusion Engineering Program
The University of Wisconsin-Madison
Madison, WI 53706 U.S.A.

January 1980

UWFDM-341

To be published in Nuclear Engineering and Design.

ABSTRACT

Two inertial confinement fusion reactor designs based upon "gas protection" of the first wall from pellet debris and X-rays are reviewed. These are the laser fusion reactor design, SOLASE, and a light ion beam cavity and first wall study conducted at the University of Wisconsin. Current status of gas protection research is reviewed. The dynamics of low pressure noble gas (xenon) for the laser fusion reactor and high pressure noble gas (argon) for the LIB fusion reactor are computed. Conclusions are drawn about the use of noble gases in these reactor designs.

1. INTRODUCTION

The energy released from the exploding pellets of inertially-confined fusion systems consists of energetic neutrons, photons, and charged particles which eventually dissipate their kinetic energies in the walls surrounding the reactor cavity. Soft X-rays and charged particles have short mean free paths in solid materials so that, if they are not attenuated before bombarding the first wall, their energy would be deposited in an extremely thin surface layer causing rapid surface heating of the first wall [1]. These pulsed photon and ion irradiations may cause excessive wall erosion by evaporation, spallation and sputtering. In addition, the wall may experience significant cyclic stresses leading to fatigue failure. The energy from the 14 MeV neutrons and high energy gammas is deposited in relatively large volumes and does not pose significant heat transfer problems. Neutron-induced damage must, of course, be assessed in conjunction with the above described problems.

As a result of this problem, the study of inertial confinement fusion (ICF) reactor design has concentrated to a large extent on methods to protect the first wall from this transient surface heat load. In fact, the wall protection scheme has always been the primary distinguishing feature between different designs. One obvious solution to the wall protection problem is to make the cavity sufficiently large to reduce the wall loading, and hence, the surface temperatures and stress levels. The economic penalties involved in the increased cavity and blanket cost ($\propto d^2$) and containment building cost ($\propto d^3$) may be significant, especially for large-yield, low-repetition-rate type systems. Hence, there is a need

for developing viable protection schemes which do not depend on size alone. Several schemes have been proposed; namely, the lithium wetted wall [2,3], the magnetically protected wall [4,5], the liquid lithium "waterfall" [6,7] or jets [8], and the gas filled cavity [9-12]. This paper deals with the gas protection concept; other protection schemes are discussed elsewhere in this issue [13].

The gas protection concept has potential application in at least two forms of ICF; laser fusion and light ion beam fusion. The basic idea is that the reactor cavity is filled with a gas at a pressure consistent with the driver type and the means by which the beams are propagated to the target. The gas will attenuate the soft X-rays and thermalize the ion debris emanating from the exploding target before they reach the first wall. It is then postulated that the energy deposited in the gas will be re-radiated to the first wall over a period of time considerably longer than the original pulse duration. Such a long pulse might then be thermally accommodated by the first wall. This means that the gas will act as a "thermal capacitor" to transform energy pulses of nanosecond duration into surface heat flux pulses of millisecond duration. This behavior is crucial to the success of the gas protection scheme.

For laser fusion systems utilizing the gas protection scheme, the gas pressure inside the cavity has a relatively narrow range (0.1 - 1.0 torr). The upper bound is limited by the ability to propagate and focus the beam onto the target while the lower bound is dictated by the need to attenuate the target debris. On the other hand, gas protection in light ion beam reactors comes as a natural consequence of the means required to

propagate the ion beams from their diodes to the target. In this fusion concept it is proposed to break down ionized channels in a background gas to serve as "renewable electrical connections" between the individual diodes and the target [14]. To meet this need it is estimated that 10-100 torr of gas is required. This is a considerably higher pressure than in the laser fusion case. Therefore, in a light ion beam (LIB) fusion reactor the first wall will be automatically protected from direct bombardment by the target debris. As will be seen later, the dynamics of the cavity gas in these two cases, low vs. high pressure, and the consequent thermal and mechanical response of the first wall will be significantly different from each other.

In this paper, two reactor designs based on the gas protection concept are described. The first is the SOLASE laser fusion reactor design developed by the University of Wisconsin [9-11] while the second is a light ion beam reactor cavity also designed at Wisconsin [15]. In addition to describing these two reactors, the paper deals with the details of cavity gas dynamics and wall response for both cases.

2. THE SOLASE LASER FUSION REACTOR DESIGN

The University of Wisconsin fusion reactor design group has completed a study of laser fusion reactor problems incorporated into a self-consistent reactor design, SOLASE [9]. The purpose of the SOLASE study is to identify and quantitatively analyze the major technological features posed by laser fusion reactors, to assess the relative advantages and prospective problems, and to guide further research. The analyses of various component operations have for the most part been carried out parametrically. This approach is necessary since a wide range of pellet materials and output characteristics may be possible. Careful analysis of the effects of these parameters on the different reactor subsystems, including synergistic effects, should guide pellet designers in their search for suitable pellets for reactor applications.

The major parameters characterizing SOLASE are listed in Table 1. The pellet yield is 150 MJ at a gain of 150 so that we employ 1 MJ of laser light on target. These parameters are representative of low-yield (~100 - 200 MJ), high repetition rate (~10 - 20 Hz) systems. In the following, the SOLASE reactor is described; the discussion will be limited to first wall protection and cavity gas dynamics. Detailed description and analyses of the other subsystems including blanket design, radiation damage and materials constraints, vacuum pumping requirements, tritium breeding and containment, compatibility of first wall and pellet materials, laser, optics, and pellet design, placement and protection of the last optical elements, pellet injection requirements, heat removal and power cycle considerations, and shielding may be found elsewhere [9].

First Wall and Cavity Design in SOLASE

A general view of the SOLASE cavity is given in Fig. 1. The cavity is spherical with a 6 m radius and is filled with a noble gas (neon or xenon) at a pressure of ~1 torr. The first wall is an integral part of the blanket which is constructed entirely from graphite. Either nuclear grade graphite or chopped-fiber type graphite composite can be used. Lithium oxide particles, 100-200 μm in diameter, flow under gravity through the blanket and serve the dual purpose of tritium breeding and heat transport. The spherical cavity is divided along longitudes into sixteen blanket segments each with a honeycomb type construction (Fig. 1). The tangential spacers parallel to the front wall allow the velocity distribution of the Li_2O particles to be tailored to match the radial heat deposition curve. The radial supports provide structural rigidity and allow impulse loadings on the front wall to be transmitted to the support structure behind the blanket.

The gas pressure in the reactor cavity must satisfy two conflicting criteria. The gas density must be low enough to insure that the laser beams will not be steered from the target by laser induced gas breakdown. On the other hand, the gas density must be sufficiently high to stop the charged particle debris and X-rays from the exploding pellet before they reach the wall. Unfortunately, the first of these limits is unknown and the second depends on the output spectra of the target which are also not well-established.

Theoretical estimates show that laser induced gas breakdown will occur at pressures of 0.1 to 1 torr for noble gases and laser intensities on the order of those required for laser fusion [9,10]. It was initially

thought that the high ionization potential of neon made it the most preferable gas because it would be least susceptible to laser induced gas breakdown. However it was concluded that the breakdown mechanism is multi-photon absorption rather than the classical electron cascade collisional ionization. The breakdown threshold intensity for the multi-photon process is so low ($\sim 10^{13}$ W/cm^3) that avoidance of breakdown is probably impossible. This removed the restriction of a gas with a very high ionization potential. An investigation of the possible effects of gas breakdown on target performance was then made. Absorption of the laser beam by inverse bremsstrahlung should not be serious at the proposed gas densities ($<10^{16}$ cm^{-3}) and the initial indication is that defocussing of the laser beam by scattering should not be a severe problem for reactor size targets, several millimeters in radius. However, beam propagation through ionizable media continues to be a subject of controversy; Sparks and Sen [16] have recently suggested that considerable beam loss could occur by enhanced Raman plasmon scattering. These uncertainties must be resolved experimentally to establish the feasibility of the gas protection concept for laser fusion applications.

For the purpose of this study, in order to investigate the dynamics of the cavity gas and the resulting first wall response, the problem has been examined parametrically. First we assume that pellets can be successfully irradiated in 0.25 torr of a noble gas such as Xe. The possibility of using other gases will then be discussed. First, we examine the thermal response of the first wall to the unattenuated X-rays. Next, we examine the gas dynamics and how the energy deposited in the gas will be re-radiated to the first wall.

A parametric study of the first wall temperature rise as a function of the blackbody temperature of the target X-rays is shown in Fig. 2. These results are obtained using a one-dimensional transient heat conduction code [1]. The X-ray energy is assumed to be instantaneously deposited in the wall. The X-ray spectrum incident on the wall is obtained by modifying the original blackbody spectrum to account for X-ray absorption in the gas. The absorption coefficients given in ref. [17] are used. The modified spectrum is divided into different energy bands; the incident photons within each band are assumed to deposit their energy in the wall exponentially. Superposition techniques are then used to determine the transient temperature history of the wall. These results show that with xenon (because of its high atomic number) as the cavity fill gas, the wall temperature rise produced by the unattenuated X-rays will be small; the main problem remains the surface heat flux radiated by the gas.

Cavity Gas Dynamics

Calculations indicate that 0.1 - 1.0 torr of xenon can stop the ion debris and X-rays for representative output spectra [18]. For this low pressure gas and the representative pellet spectra, the ions' and photons' energy will not be deposited in a small volume surrounding the pellet but will be distributed through the gas in some profile that may extend to the first wall. Analysis of the gas response to this energy deposition is quite important since it must retain this energy and re-radiate it to the first wall in a long pulse (~msec). This is the key element of the gas protection scheme proposed in the SOLASE laser fusion reactor study. The analysis has been performed using the fireball code FIRE developed at the University of Wisconsin [19,20].

In Table 2 we present the results of a calculation for 0.25 torr of xenon in a 6 meter cavity with a deposited energy of 30 MJ. This energy is assumed to be uniformly deposited in a 1 meter sphere surrounding the pellet. These results might be considered to correspond to the SOLASE reactor cavity situation. The heat flux and overpressure experienced at the first wall are shown in Fig. 3. The average heat flux, computed as the energy radiated to the wall in the high intensity part of the pulse divided by the width of this pulse, is 40.2 kW/cm^2. This heat flux is much higher than the estimate used in the SOLASE study and leads to a temperature rise in the first wall of 1740°C. However, the overpressure experienced at the wall is very low, 14 torr. This is lower than the design value in SOLASE.

The reason for this very large heat flux can be learned from studying the plasma and radiation temperature profiles in the xenon gas along with the radiation mean free path. A snapshot plot of these is given in Fig. 4 at a time of 0.65 μs. In this low pressure case the radiation mean free path in the hot fireball is very long and the mean free path in the surrounding cold gas is very long. However, in the temperature gradient between these two, there is a region of plasma where the mean free path is short. This is at a radius of about 400 cm in the snapshot shown in Fig. 4. This opaque region of plasma prevents the radiation behind it from streaming to the first wall. Note that the radiation temperature in the fireball has nearly come into equilibrium with this plasma region at a temperature of 2 eV, while the plasma temperature in the fireball is still 5-10 eV. This decoupling of the temperatures points out the importance of

the two temperature model used in these calculations. This situation continues until this opaque plasma region has propagated to the first wall, at 2.8 μs. At this time the first wall is almost instantaneously exposed to all of the hot plasma behind this barrier; the fireball volumetrically radiates to the first wall. This results in a very large instantaneous heat flux. The heat flux decays very quickly because the fireball is rapidly losing energy and its temperature is dropping. Thus in this example the cavity gas retains the explosion energy until the thermal wave created by the energy deposition reaches the first wall. Then the energy is rapidly radiated to the first wall.

The rapid energy release by the gas results in high temperature excursions at the first wall surface. A parametric study has been conducted to determine the relation between the re-radiation pulse width and the wall thermal response [1]. The radiant heat flux incident on the first wall is assumed to either remain constant over a period $\beta\omega$, where ω is the time between pulses, or drop exponentially from a maximum value at the beginning of each pulse. The parameter β or the time constant for the exponential decay is then varied and the thermal response of a finite slab of thickness L subjected to a sequence of these heat flux pulses is obtained [1]. The back surface of the slab is assumed to remain at a constant temperature since the first wall (or blanket face) will be actively cooled.

Typical results showing the surface temperature rise in a graphite wall subjected to a train of heat flux pulses with average wall fluxes (averaged over entire period between pulses w) of 150 W/cm^2 for both heat flux distributions are shown in Figs. 5 and 6. These results do not

account for any evaporation which may take place at the surface. It is obvious that the surface temperature rise, and hence the maximum surface temperature, will decrease as the pulse width is increased. For the case shown, which roughly corresponds to the SOLASE design, in order to prevent excessive evaporation and spallation of the wall, the energy deposited in the gas must be radiated over a period $\geq \sim 1$ ms, i.e., the maximum instantaneous heat flux should be less than ~5.0 kW/cm^2. This is considerably lower than the computed value of 40 kW/cm^2 for 0.25 torr xenon in the cavity.

The rather special set of circumstances that lead to this result casts doubt on the general applicability of this behavior over the range of uncertainties associated with the fireball creation process. The initial conditions are of course determined by the pellet output spectra. This problem is studied parametrically by assuming that the pellet energy is deposited in spheres of radii 1 meter, 3 meters, and 5 meters surrounding the pellet. The results of all of these calculations are presented in Table 3 for a 30 MJ charged particle and X-ray yield and 0.25 torr of xenon in a 6 meter cavity. As the initial fireball radius becomes larger, the amount of energy radiated to the wall increases but the time over which this energy is radiated also increases substantially. Hence the average heat flux incident on the wall decreases with increasing fireball radius. However, this heat flux is still substantial and the gas displays the same characteristics in all three cases. It only holds the deposited energy for about 0.1 msec whereas the graphite wall designs require a re-radiation time of greater than 1.0 msec.

Numerous calculations for different pellet yields and cavity sizes have also been made [19]. These results indicate that for target yields of 100-1000 MJ, cavity radii of 6-12 m, initial fireball radii of 1-5 m and a gas pressure of 0.25 torr when measured at 0°C, inert cavity gases do not act as a thermal capacitor to hold up the energy of the microexplosion. Large instantaneous heat fluxes on the first wall lead to unacceptable temperature transients and thermal stress levels. At the low pressures expected in laser fusion cavities, the radiation mean free paths in the fireball and outside the fireball are long. The mean free paths in the temperature gradient between hot and cold regions are short. Consequently, the fireball does not drive a shock wave to the first wall, but instead a supersonic thermal wave propagates through a motionless gas. Once this opaque region of plasma in the temperature gradient reaches its transparency temperature, the fireball volumetrically radiates to the first wall. This combination of effects results in very high instantaneous heat fluxes but very low overpressures at the first wall.

These results clearly indicate that noble gases in the pressure range of 0.1-1.0 torr are unacceptable for protecting the first wall of laser fusion reactors. Furthermore, if the gas pressure could be raised to 1-10 torr the basic conclusions would likely be the same. However, these conclusions are closely linked to the properties of noble gases. The radiative properties of diatomic gases are considerably different and could completely change these conclusions. Recall that the choice of a noble gas was made because of fear that the laser beams would break down the gas before reaching the target and this would spoil the target irradiation. Hence the viability of the gas protection scheme in laser

fusion depends on both the choice of a gas with proper radiative properties and the ability of this gas to transmit the laser beams without catastrophic breakdown problems.

3. GAS PROTECTION IN LIGHT ION BEAM FUSION CAVITIES

For the last several years, fusion reactor design work in support of the particle beam fusion program has been conducted at Sandia Laboratories [12]. Most recently, collaboration between Sandia and the University of Wisconsin Fusion Engineering Program have yielded the most detailed cavity design studies for LIB reactors [15]. The results of these studies are reviewed in this part of the paper.

No complete conceptual design of a light ion beam fusion reactor (such as the SOLASE design for laser fusion) has been undertaken. However, there has been significant work in the areas of cavity and first wall design. A possible LIB fusion reactor design is shown in Fig. 7. In this design the spherical cavity is surrounded by a first wall of stainless steel panels that are supported from behind by a structural frame. This frame is shown more clearly in Fig. 8. Gas is injected at the top of the cavity and the hot gas, following the microexplosion, is pumped out through the large duct at the bottom of the cavity. The light ion beam transmission lines and diodes penetrate the blanket as shown in Fig. 7. The ion beams are transported from the final diodes to the target through ionized channels that are formed by laser ionization of the cavity gas [14]. Hence, gas protection of the first wall in a LIB reactor comes as a natural consequence of the beam propagation mode. The ionized channels in the cavity gas serve as "renewable electrical connections" between the individual diodes and the target. To meet this need it is estimated that a gas density of 3×10^{17} -- 3×10^{18} cm^{-3}, or 10-100 torr measured at 0°C, will be required. This is a considerably higher pressure than in the laser fusion case and all gases but the very lightest, He and H, will

effectively stop the target debris and X-rays before they reach the first wall. In fact, the gas will stop them in a small volume surrounding the target, thus creating a fireball. This fireball subsequently expands, driving a shock ahead of it to the first wall. A significant overpressure is experienced at the first wall when the shock front is reflected. Therefore the first wall must be constructed from a strong structural material and must have an appreciable thickness. The first wall material receiving the most attention thus far is 316 stainless steel. A cellular wall design, as shown in Fig. 8, adds stiffness to the wall without adding to its weight or effective thickness to neutrons. Possible parameters for a light ion beam fusion reactor are given in Table 4.

The necessary strength of the first wall adds constraints to its design in terms of materials choice and thickness. These must be sufficient to meet the large overpressures of several atmospheres on a repetitive basis without exceeding maximum stress criteria. However, this poses problems for the thermal response of the wall to the radiating fireball. Although the cellular wall design allows the flowing of coolant in the internal channels, the front face of the cellular wall is still 0.5 - 1 cm thick. This places severe constraints on the radiative characteristics of the gas. It is clearly desirable that the gas radiate its energy to the wall in a long pulse but not so long that it fails to cool before the next pulse. If this is the case, then the gas must be pumped from the cavity and cooled in an external heat exchanger. Furthermore, the radiative properties of the fireball are strongly dependent

on the type of cavity gas. We next review the response of noble gases at 50 torr pressure to the exploding target X-rays and debris.

Initially, noble gases seemed to be a good choice due to their inertness, and hence compatibility with almost any first wall material and the pellet debris. Medium atomic number gases such as argon or neon were also preferred because they were more suitable for the ion beam transport in ionized channels. It is thought that the dominant energy loss mechanism in the channels is classical ion scattering which is greater for high Z gases as shown in Table 5. Hence the choice of xenon for LIB cavities is not likely to be acceptable.

To compute the fireball dynamics we postulate that the pellet explosion will almost instantaneously put the cavity gas in an initial state characterized by a hot ball of plasma with a radius of ~10 cm at the center of the cavity, surrounded by cold gas out to the first wall. This model is certainly an idealization of the actual dynamics of the pellet exploding into the gas immediately surrounding it. However, since we expect that the propagation of the pellet energy obeys something resembling strong shock theory, the only important initial parameters should be the energy and the mass density. Using this model for the initial condition of the fireball we compute its dynamic behavior using the FIRE hydrodynamics code [20]. The pellet mass is added to the cavity gas mass (only one ion specie is allowed in the FIRE code) and is uniformly distributed in the 10 cm initial fireball. The details of a representative calculation are given in Table 6. The 30 MJ of yield that is deposited in the gas corresponds to a total yield of 100-150 MJ when the 14.1 MeV neutrons are included. This is a range of

yield that is considered for light ion beam driven targets. Figure 9 is a plot of the plasma temperature profiles in the plasma as a function of radius at different times during the shock propagation to the wall. Figure 10 is a similar plot of the pressure. Figure 11 is a plot of the heat flux and mechanical overpressure experienced at the first wall as a function of time and Fig. 12 is a plot of the Planck and Rosseland averaged radiation mean free paths as functions of the plasma and radiation temperatures when they are equal. Figure 12 shows that the argon plasma becomes transparent to its equilibrium radiation at a temperature of ~1 eV. Figure 9 shows that the fireball reaches this temperature at a time between 0.1 ms and 0.46 ms after the fireball creation and Fig. 11 indicates that this is when the first wall experiences the heat flux leaking from the fireball. Figures 9 and 10 show that the shock has separated from the fireball by 0.46 ms and propagates to the wall by itself. Figure 13 is an R-t plot of the gas motion. Each line in this plot follows the trajectory of a unit of mass as a function of time. The shock can be clearly seen as a bunching of the lines. The prediction of strong shock theory is also plotted on Fig. 13 and we see that the shock speed begins to deviate from strong shock theory early in time. The heat flux at the wall averaged over the pulse width is 15 kW/cm^2. This is unacceptably large for reactor applications. The resultant temperature rise in a 0.5 cm stainless steel wall is 317°C when the repetition rate is 10 Hz. The temperature transient is shown in Fig. 14.

All of these results are attributable to the high transparency of low energy photons in argon. Air, for instance, has a transparency temperature of 0.2 eV. The high transparency of argon at temperatures below 1 eV is due to the monatomic nature of the molecule. Electronic transitions are the lowest transitions available to strongly absorb a photon and the lowest electronic transition energy is very high for noble gases, 16 eV for argon. Hence, photons below about 16 eV are only weakly absorbed. This situation is much different for polyatomic molecules where the rotational and vibrational transitions are available to absorb low energy photons or other monatomic gases with lower ionization potentials. These gases are much less transparent to low energy photons and transparency temperatures are much lower. To demonstrate the importance of this point, the argon data used in the example calculation is modified so that the radiation mean free path below 1.5 eV is limited to no greater than 50 cm. This gas we call "diatomic argon". The results of an identical calculation using this gas are also given in Table 6 and are displayed in Fig. 15. From Fig. 15 we see that the heat flux comes only after the pressure pulse has hit the first wall and the maximum heat flux is only 0.12 kW/cm^2. The resulting surface temperature rise is only 3°C. On the other hand, the overpressure is greater in this case because energy is never leaked from the fireball before the shock arrives at the wall. This comparison verifies the assertion that the high transparency of noble gases at low temperature leads to the premature release of the radiant energy in the fireball. Therefore, a strong distinction exists between the behavior of noble and non-noble gases in high pressure reactor cavities.

These results also lead to the conclusion that the gas in a LIB cavity can be tailored to have the correct radiative properties and hence radiate its energy to the wall in controlled pulses of sufficiently long duration to avoid excessive temperature transients. Such a tailoring process could be accomplished by mixing gases of differing properties, as demonstrated by the two limiting cases given as examples. This will be discussed more fully in part 4.

4. CURRENT STATUS AND CONCLUSIONS

Parts 2 and 3 of this paper have been devoted to reviews of a laser fusion conceptual reactor design (SOLASE) and a light ion beam fusion cavity and first wall design, both based on gas protection of the first wall from the pellet debris and X-rays. The results presented here are predicated on the best physical model of gas response that is available. From a historical perspective, the SOLASE study was concluded two years before the calculations presented here were done. This explains the inconsistency between the conclusions drawn in the original SOLASE study and those drawn in this review. The LIB results are very recent and represent only the first attempt at a detailed cavity design. Hence further inprovements in this design are already underway.

The physical model of the gas response normally takes the form of a radiation-hydrodynamics computer code. At least three such codes are operational, CHART-D [21], FIRE [20], and multi-frequency CHART-D [22]. In ascending degrees of accuracy these codes simulate the hydrodynamic response and radiative energy transfer in the cavity gas. These simulations give the mechanical overpressure and radiant heat flux experienced by the first wall. The wall response can then be computed from these input quantities.

A very important aspect of this problem are the physical properties of the cavity gas. These are used as input to the hydrodynamics codes. Such properties are not readily available because there has been little need for such properties in the temperature (0.1-100 eV) and density (3×10^{14}-3×10^{18} cm^{-3}) ranges of interest. (The exception to this is air,

where the nuclear weapons program has required these properties.) Currently, the research on cavity gas response is paced by the calculation of these gas properties. In the last year the properties of noble gases have been computed to an acceptable degree of accuracy [23]. This in fact partially explains the choice of noble gases in the two reviewed studies. These monoatomic gases may represent the simplest molecule to analyze. The next simplest system may be a mixture of two such monatomic gases. Mixtures of this kind are particularly important to LIB fusion where it has been recently postulated that a combination of 50 torr of argon and 1 torr of an alkali metal vapor such as sodium, will allow very efficient channel formation by laser ionization [24]. Work is currently underway at the University of Wisconsin to compute the properties of these monatomic gas mixtures. Preliminary results show that this gas mixture will have a lower transparency temperature and will likely have the proper response for reactor applications as outlined in part 3.

The properties of polyatomic gases are difficult to compute because of the additional transitions between rotational and vibrational states in the molecule. Monatomic gases only require computation of photon absorption and emission due to electronic transitions. The addition of vibrational and rotational transitions will increase the gas opacity at low temperatures, thus again possibly avoiding the burst of fireball energy to the wall that is predicted for noble gases. The use of polyatomic gases may be the only possibility for the laser fusion application of gas protection. The choice of a polyatomic gas will also depend on its chemical

compatibility with the wall and with the target debris. But most importantly, it must allow the transmission of the laser beams to the target. A large number of gas breakdown studies have been done but the results are very dependent on the particular experimental conditions. Therefore the applicability of polyatomic gases must first be tested by appropriate gas breakdown experiments.

Most gas response calculations to date have assumed that the pellet X-rays and debris are instantaneously deposited into the gas. Some calculations [25] lead to the speculation that such an approximation may not be strictly correct and that the subsequent gas response is dependent on the dynamics of the X-ray and ion deposition in the gas. This may be particularly true in the case of laser fusion where the pellet X-rays and debris are stopped in a large volume of low pressure gas. This problem was identified by both Sandia and the University of Wisconsin and work is currently underway to resolve this question.

In conclusion, the gas protection concept for laser fusion reactors has passed through an oscillation of high, low, and medium confidence. Its viability today rests upon the transparency of polyatomic gases to high intensity laser light. In the LIB case, there are fewer constraints on the cavity gas. Pure noble gases appear to be ruled out, but mixtures of noble gas and another gas such as sodium vapor seem to have many desirable properties.

Acknowledgment

Partial support has been provided by the Electric Power Research Institute, and by Sandia Laboratories.

References

1. S. I. Abdel-Khalik and T. O. Hunter, "Assessment of Surface Heating Problems in Laser Fusion Reactors," UWFDM-197, University of Wisconsin (July 1977), J. Heat Transfer, 100, 311 (1978).

2. L. A. Booth, (compiler), "Central Station Power Generation by Laser-Driven Fusion", Los Alamos Scientific Laboratory, LA-4858-MS (1972).

3. J. M. Williams, et al., "A Conceptual Laser Controlled Thermonuclear Reactor Power Plant", Proc. 1st Topical Meeting on the Technology of Controlled Nuclear Fusion, San Diego (1974).

4. L. A. Booth and T. G. Frank, "A Technology Assessment of Laser-Fusion Power Development", Los Alamos Scientific Laboratory Report LA-UR-2060, presented at the Second ANS Topical Meeting on the Technology of Controlled Nuclear Fusion, Richland (Sept. 1976).

5. D. A. Freiwald, T. G. Frank, E. A. Kern, and L. A. Booth, "Laser Fusion Generating Stations Based on the Magnetically Protected Reactor Cavity", Los Alamos Scientific Laboratory Report LA-UR-75-2035; also Trans. ANS, 22, 68 (1975).

6. J. A. Maniscalco and W. R. Meier, "Liquid-Lithium 'Waterfall' Inertial Confinement Fusion Reactor Concept", Trans. ANS, 26, 62 (1977).

7. J. Powell, et al., "A Liquid-Wall Boiler and Moderator (BAM) for Heavy Ion-Pellet Fusion Reactors", Trans. ANS, 26, 64 (1977).

8. M. Monsler, et al., "Electric Power from Laser Fusion: The HYLIFE Concept", Trans. ANS 30, 21 (1978).

9. R. W. Conn, et al., "SOLASE, A Laser Fusion Reactor Study", University of Wisconsin Fusion Engineering Program Report UWFDM-220 (1977).

10. G. A. Moses, et al., "The SOLASE Conceptual Laser Fusion Reactor Study", Proc. 3rd ANS Top. Meeting on the Technology of Controlled Nuclear Fusion, CONF-780508, Vol. 1, 448, Santa Fe (May 1978).

11. S. I. Abdel-Khalik, et al., "Engineering Problems of Laser Driven Fusion Reactors", Nucl. Tech. 43, 5 (1979).

12. D. L. Cook and M. A. Sweeney, "Design of Compact Particle Beam Driven Fusion Reactors", Proc. 3rd ANS Top. Meeting on the Technology of Controlled Nuclear Fusion, CONF-780508, Vol. 2, 1178, Santa Fe (May 1978).

13. M. Monsler, et al., "Inertial Confinement Reactors Based Upon Lithium Falls", Nucl. Eng. Design (this issue).

14. G. Yonas, "Fusion Power with Particle Beams", Sci. Am. 239, 50 (Nov. 1978).

15. G. A. Moses, S. I. Abdel-Khalik, et al., "First Wall and Cavity Design Studies for a Light Ion Beam Driven Fusion Reactor", University of Wisconsin Fusion Engineering Program Report UWFDM-320 (1979).

16. M. Sparks and P. N. Sen, "Possible Reduction of Laser-Fusion Target Illumination by Enhanced Stimulated Raman Plasmon Scattering", Phys. Rev. Lett., 39, 751 (1977).

17. F. Biggs and R. Lighthill, "Analytical Approximations for X-ray Cross Sections II", SC-RR-0507, Sandia Laboratories (1971).

18. T. O. Hunter and G. L. Kulcinski, "Description of the Response of Material to Pulsed Thermonuclear Radiation - Effect of Gases on Modification of Pellet Debris Spectra and First Wall Response", University of Wisconsin Fusion Engineering Report UWFDM-232, (April 1978).

19. G. A. Moses and R. R. Peterson, "First Wall Protection in ICF Reactors by Inert Cavity Gases", University of Wisconsin Fusion Engineering Program Report UWFDM-323 (October 1979). (Submitted for publication to Nuclear Fusion.)

20. G. A. Moses and R. R. Peterson, "FIRE-A Computer Code to Simulate Cavity Gas Response to Inertial Confinement Target Explosions", University of Wisconsin Fusion Engineering Program Report UWFDM-336 (January 1980).

21. S. L. Thompson, "Improvements in the CHART-D Energy Flow Hydrodynamic Code V: 1972/73 Modifications", SLA-73-0477, Sandia Laboratories (1973).

22. L. Baker, "CHART-B Multigroup Transport Package", Sandia Laboratory Report SAND-79-0386, March 1979.

23. R. R. Peterson and G. A. Moses, "MFP - A Calculation of Radiation Mean Free Paths, Ionization and Internal Energies in Noble Gases," University of Wisconsin Fusion Engineering Program Report UWFDM-307 (September 1979). (Submitted for publication to Computer Physics Communications.)

24. G. W. Cooper, private communication, Jan. 1979. (See also, R. M. Measures, N. Drewell, and P. Cardinal, "Electron and Ion-Beam Transportation Channel Formation by Laser Ionization Based on Resonance Saturation-LIBORS", J. Appl. Phys. 50 (4), 2262 (1979)).

25. M. A. Sweeney and D. L. Cook, "Blast-Wave Kinetics and Thermal Transport in a Particle-Beam Reactor Chamber", Bull. APS 24, 1072 (1979).

Table 1

Major Parameters of SOLASE

Cavity Shape	Spherical
Cavity Radius	6 m
Laser Energy on Target	1 MJ
Maximum Laser Power on Target	1000 TW
Pellet Yield	150 MJ
Pulse Rep. Rate	20 Hz
Estimated Overall Laser Efficiency	7%
Number of Final Mirrors	12
Distance from Last Mirror to Target	15 m
Diameter of Last Mirror	3.5 m
Composition of Last Mirror	Cu on Al
Neutron Wall Loading	5 MW/m^2
Tritium Breeding Ratio	1.34
Total Energy Per Fusion Event	2.98 pJ (18.6 MeV)
Blanket Structure	Graphite
Blanket Breeding and Heat Transport Medium	Lithium Oxide
Li_2O Inlet Temp.	673^oK
Li_2O Outlet Temp.	873^oK
Average Li_2O Flow Velocity	0.4 m/s
Total Li_2O Flow Rate	8.67×10^3 kg/s
Power Cycle	Li_2O-Stream
Total Thermal Power Output	3190 MW(th)
Estimated Gross Electrical Output	1335 MWe
Estimated Net Electrical Output	1000 MWe
Estimated Net Plant Efficiency	30%

Table 2

Fireball Calculation of 1/4 torr
of Xenon in a 6 meter Cavity

Cavity Radius	6 meter
Gas Type	Xe
Gas Pressure (0°C)	0.25 torr
Energy Deposited	30 MJ
Initial Fireball Radius	1 meter
Initial Fireball Temperature	23.5 eV
Initial Gas Temperature	0.1 eV
Maximum Overpressure	13.7 torr
Time of Maximum Overpressure	23 μs
Energy Radiated to First Wall*	10 MJ
Average Heat Flux**	40.2 kW/cm^2
Pulse Width**	55 μs

* The energy radiated to the wall is defined as the amount of energy radiated for instantaneous values of the heat flux greater than 10% of the maximum.

** The average heat flux is defined as the energy radiated to the first wall divided by the pulse width.

Table 3

Comparison of 1, 3, and 5 m Fireballs for a 30 MJ Fireball in 1/4 torr of Xenon

	Fireball Radius		
	1 m	3 m	5 m
Cavity Radius (m)	6	6	6
Gas Type	Xe	Xe	Xe
Gas Pressure (0°C) (torr)	0.25	0.25	0.25
Energy Deposited (MJ)	30	30	30
Initial Fireball Temperature (eV)	23.5	4.5	2.0
Initial Gas Temperature (eV)	0.1	0.1	0.1
Maximum Overpressure (torr)	13.7	15.2	18.2
Time of Maximum Overpressure (μs)	23	25	1000
Energy Radiated to First Wall*(MJ)	10	14.5	14.7
Average Heat Flux**(kW/cm^2)	40.2	25.6	18.5
Pulse Width**(μs)	55	125	175

*The energy radiated to the first wall is defined as the amount of energy radiated for instantaneous values of the heat flux greater than 10% of the maximum.

**The average heat flux is defined as the energy radiated to the first wall divided by the pulse width.

Table 4

Possible Parameters for a Light Ion Beam Fusion Reactor

Cavity Shape		Spherical
Cavity Radius		4 meters
Cavity Gas		50 torr Ar + 1 torr Na
First Wall Material		Stainless Steel
Number of First Wall Panels		32/hemisphere
Panel Dimensions	Height	420 cm
	Width	78.5 cm
	Thickness	5.6 cm
	Cell Wall Thickness	0.5 cm
Maximum Stress Limit		20 ksi
Target Yield		100 MJ
Yield in X-rays and Ions		30 MJ
Repetition Rate		10 Hz
Total Power		1000 MW_t
Overpressure at First Wall		4 atm

Table 5

Energy Loss of Protons in a 4 meter Long
Plasma Channel of Density = 10/760 Atmospheric
(Corresponds to 50 torr Chamber Prefill)

Gas	Energy Loss for 2 MeV Proton (MeV)	Energy Loss for 4 MeV Proton (MeV)	Energy Loss for 10 MeV Proton (MeV)
He	0.16	0.09	0.04
Li	0.24	0.14	0.07
N_2	0.90	0.55	0.26
Ne	0.55	0.36	0.18
Ar	0.90	0.55	0.28
Xe	1.80	1.20	0.65

Table 6

Input Parameters for FIRE Calculations

	Gas Type	
	Argon	Diatomic Argon
Cavity radius (m)	4	4
Gas pressure at 0°C (torr)	50	50
Gas number density (cm^{-3})	1.67×10^{18}	1.67×10^{18}
Gas mass density (g/cm^3)	1.114×10^{-4}	1.114×10^{-4}
Energy deposited in fireball (MJ)	30	30
Initial fireball radius (cm)	10	10
Initial fireball temperature (eV)	64	64
Initial fireball charge state	12	12
Maximum overpressure (atm)	1.5	2.75
Time of maximum overpressure (ms)	2.3	1.7
Energy radiated to wall (MJ)	7.5	0.15
Average heat flux* (kW/cm^2)	15	0.05
Pulse Width* (μs)	110	1500

* The average heat flux is defined as the energy radiated to the first wall divided by the pulse width.

Figure Captions

Fig. 1: Schematic Diagram of the SOLASE Reactor Cavity Showing Detailed Blanket Construction.

Fig. 2: Variation of the Wall Temperature Rise Produced by the Unattenuated X-rays as a Function of the Blackbody Temperature of the Original Spectrum.

Fig. 3: Time-Dependent Pressure and Heat Flux at the First Wall for 30 MJ of X-ray and Ion Energy Deposited in 0.25 torr Xenon-Filled Cavity.

Fig. 4: Variation of the Plasma and Radiation Temperatures and the Planck Mean Free Path at 0.65 μs after the Explosion for the Case Shown in Fig. 3.

Fig. 5: Variation of the Temperature Rise Produced in a Graphite Wall by a Train of Square Heat Flux Pulses with Pulse Width (T_{max} and $\Delta T_{surface}$ are the Maximum Surface Temperature and Temperature Rise Respectively).

Fig. 6: Results Similar to Those in Fig. 5 for a Series of Exponentially Decaying Heat Flux Pulses ($t_{1\%}$ is the Time Required for the Surface Heat Flux to Drop to 1% of its Maximum Value).

Fig. 7: Schematic Diagram of a Light Ion Beam Reactor Cavity and First Wall.

Fig. 8: Design of Cellular First Wall Supported by a Structural Frame.

Fig. 9: Gas Temperature Profiles at Various Times for a 30 MJ Explosion in 1.67×10^{18} cm^{-3}, 0.1 eV Argon Gas.

Fig. 10: Gas Pressure Profiles at Various Times for the Case Shown in Fig. 9.

Fig. 11: Pressure and Heat Flux at a 4 meter Radius First Wall for the Case Shown in Fig. 9.

Fig. 12: Rosseland and Planck Mean Free Paths for Radiation in 1.67×10^{18} cm^{-3} Argon. The Radiation is Assumed to be in Equilibrium with the Gas so that $T_p = T_R = T$.

Fig. 13: Propagation of a Shock for the Case Shown in Fig. 9. The Positions of the Boundaries of 50 Lagrangian Zones are Plotted Against Time as is the Position of the Shock Front Predicted by Strong Shock (Taylor-Sedov) Theory.

Fig. 14: Transient Temperatures for a 0.5 cm Thick Stainless Steel First Wall Experiencing the Heat Flux Shown in Fig. 11.

Fig. 15: Pressure and Heat Flux for the Case of "Diatomic Argon". The Radiation Mean Free Paths are those of Argon except when $T_R <$ 1.5 eV, Where They are no Larger than 50 cm.

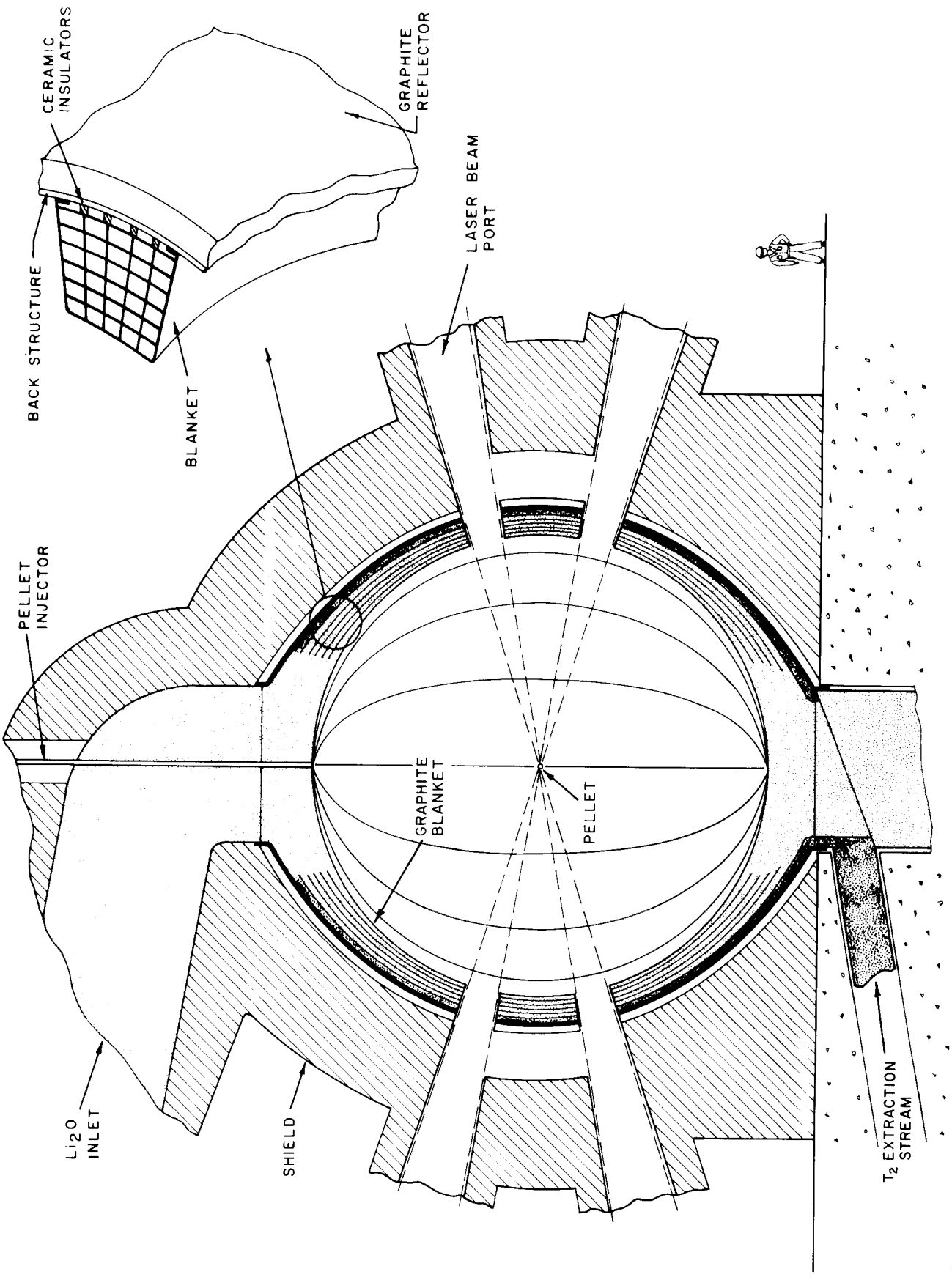
CERAMIC INSULATORS
GRAPHITE REFLECTOR
BACK STRUCTURE
BLANKET
LASER BEAM PORT
PELLET INJECTOR
GRAPHITE BLANKET
PELLET
Li_2O INLET
SHIELD
T_2 EXTRACTION STREAM

FIGURE 1

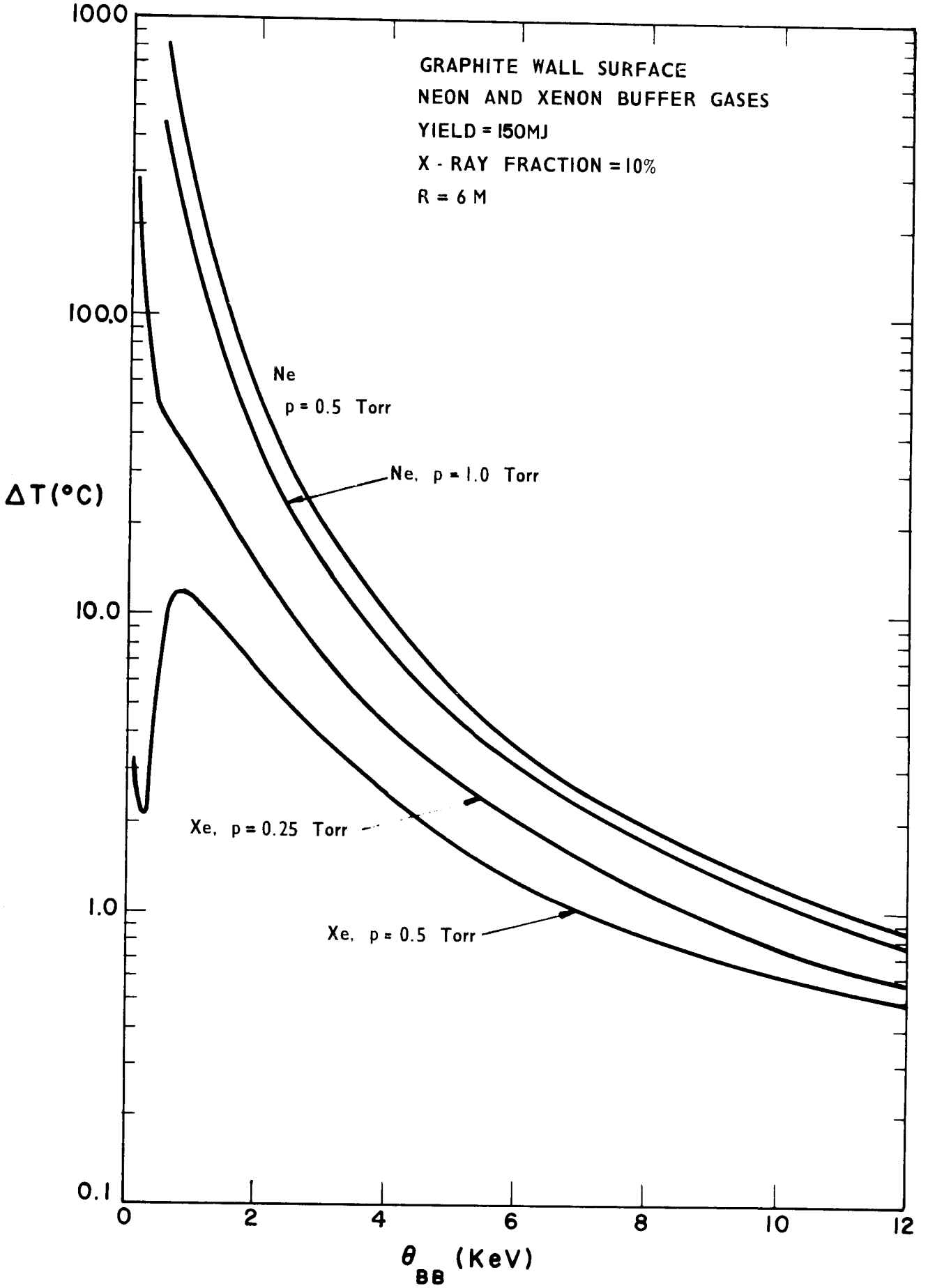
GRAPHITE WALL SURFACE
NEON AND XENON BUFFER GASES
YIELD = 150MJ
X - RAY FRACTION = 10%
R = 6 M
Ne
p = 0.5 Torr
Ne, p = 1.0 Torr
Xe, p = 0.25 Torr
Xe, p = 0.5 Torr
ΔT(°C)
1000
100.0
10.0
1.0
0.1
0
2
4
6
8
10
12
θBB (KeV)

FIGURE 2

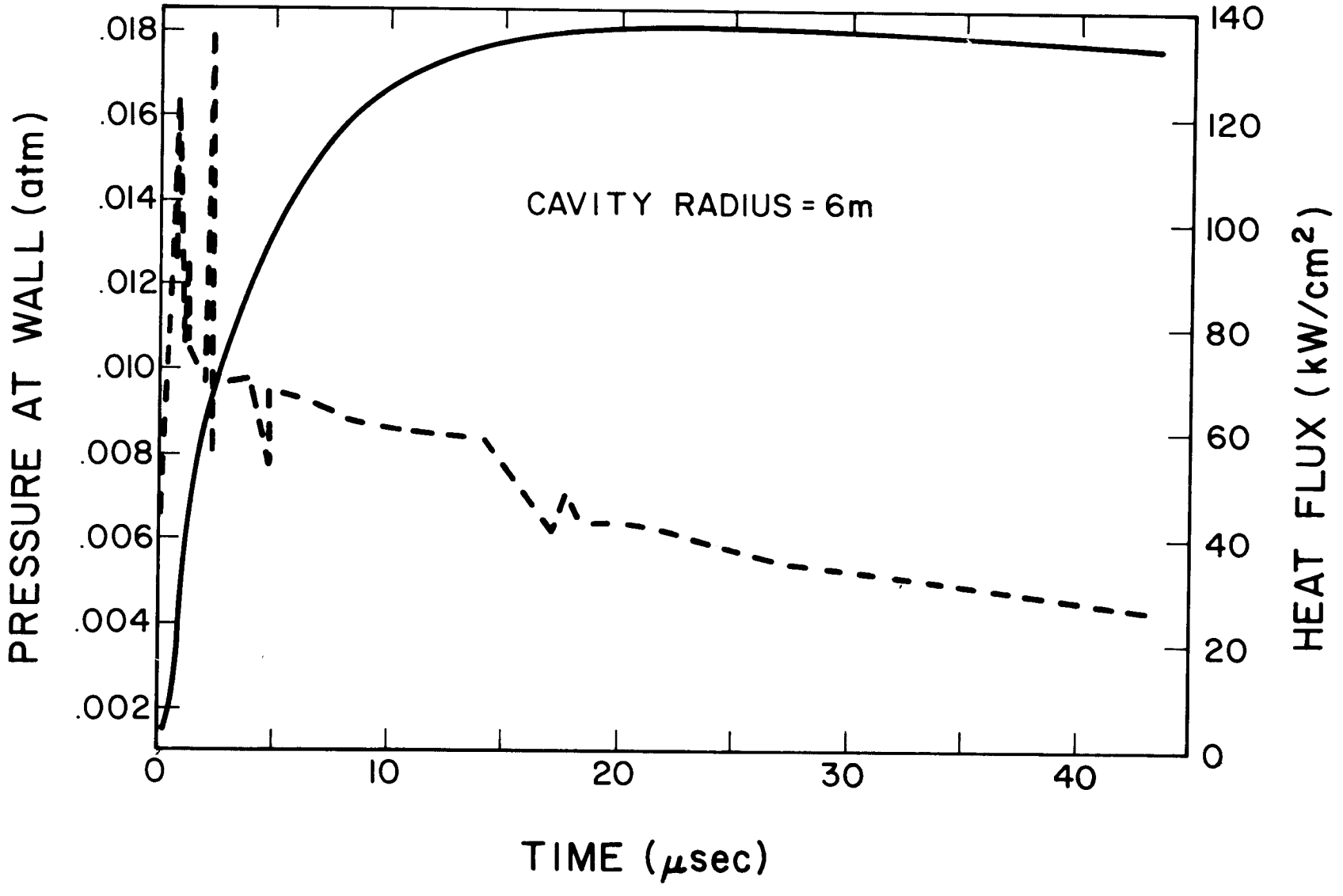
PRESSURE AND HEAT FLUX AT FIRST WALL FOR
30 MJ EXPLOSION IN 0.25 TORR XENON
CAVITY RADIUS = 6m
PRESSURE AT WALL (atm)
.018
.016
.014
.012
.010
.008
.006
.004
.002
HEAT FLUX (kW/cm2)
140
120
100
80
60
40
20
0
0
10
20
30
40
TIME (μsec)

FIGURE 3

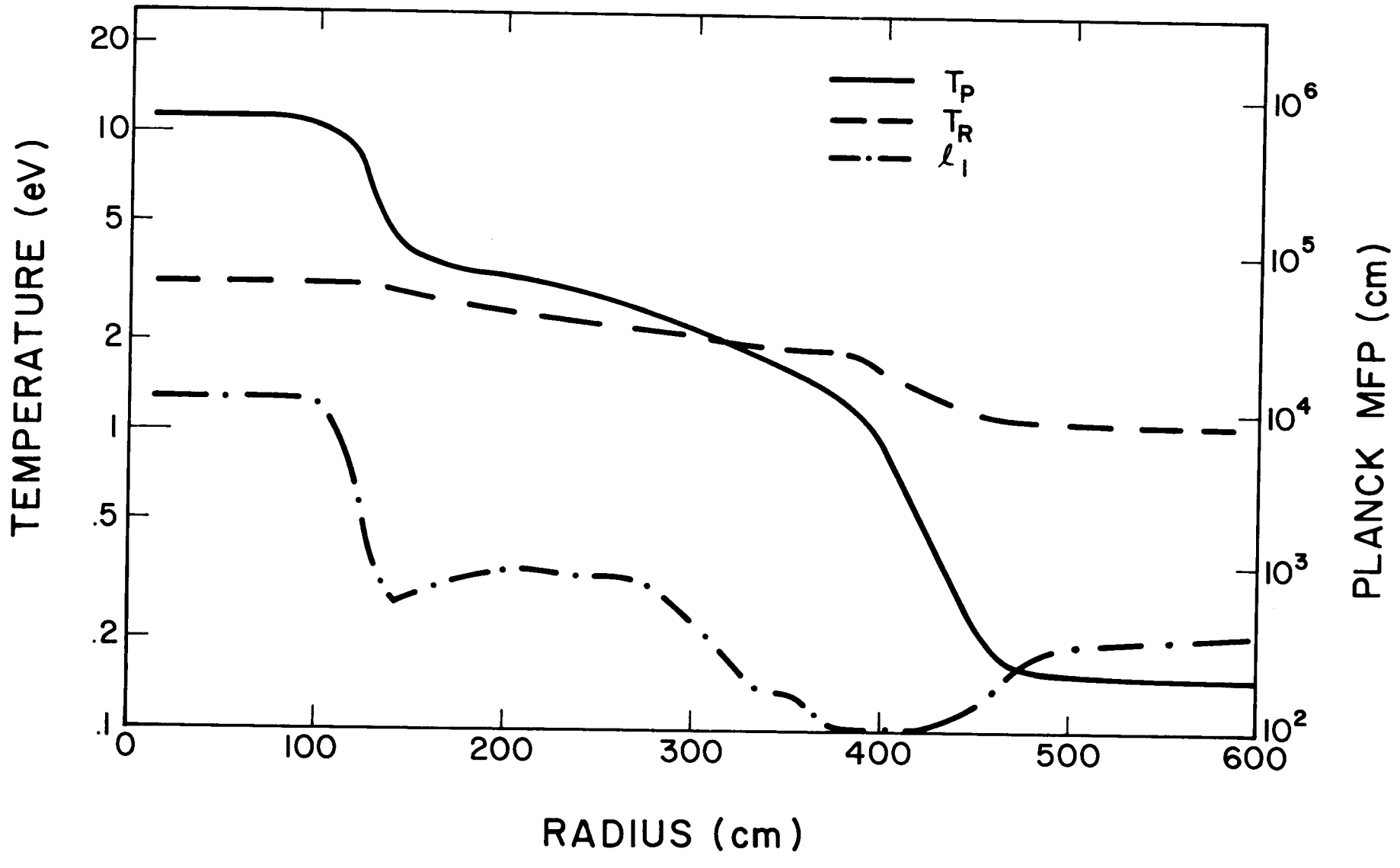
PLASMA TEMPERATURE, RADIATION TEMPERATURE, AND PLANCK MFP AT 0.65 μs FOR 30 MJ EXPLOSION IN 0.25 TORR OF XENON
TEMPERATURE (eV)
20
10
5
2
1
.5
.2
.1
T_P
T_R
ℓ_1
10^6
10^5
10^4
10^3
10^2
PLANCK MFP (cm)
0
100
200
300
400
500
600
RADIUS (cm)

FIGURE 4

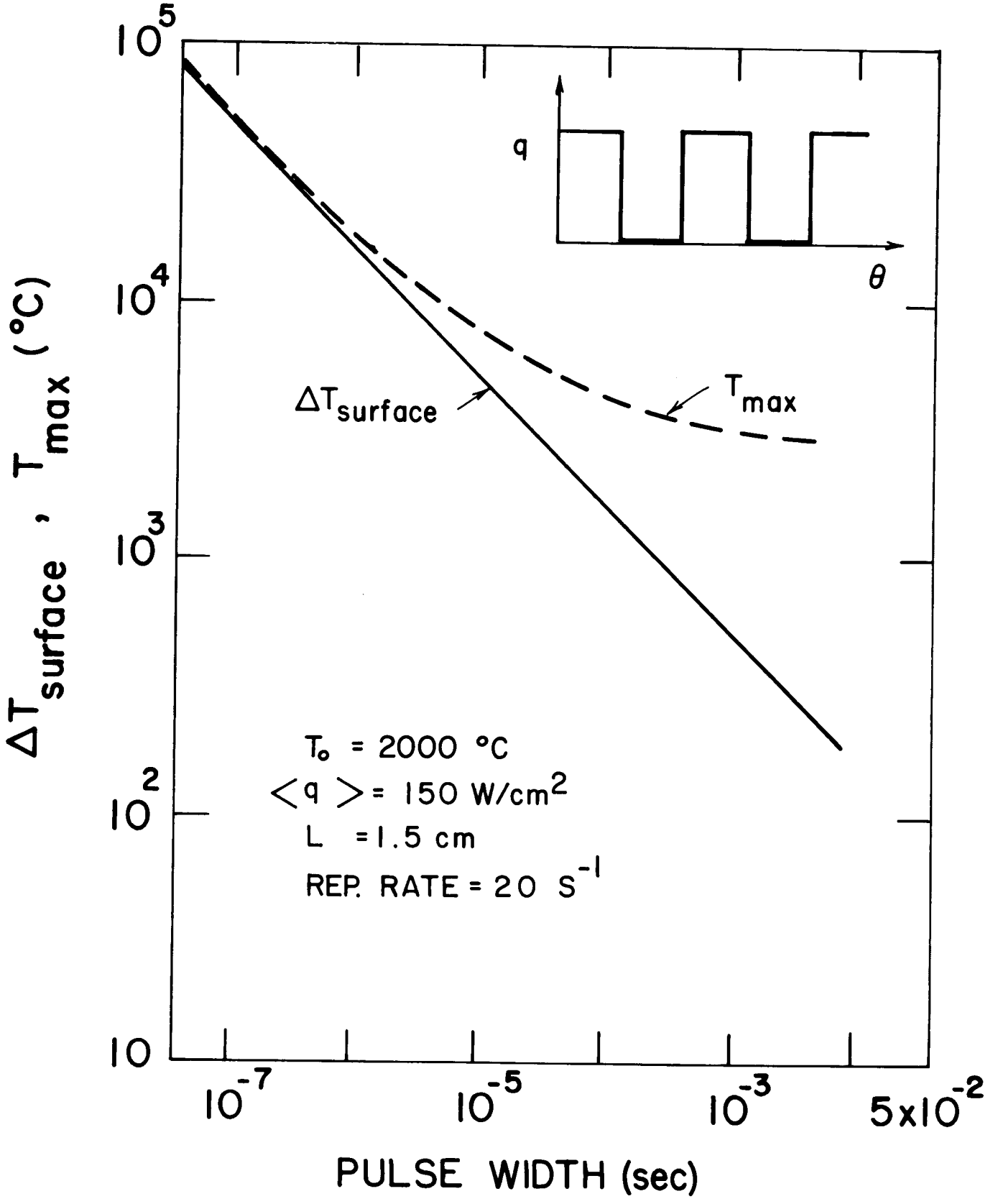
10^5
10^4
10^3
10^2
10
$\Delta T_{surface}$, T_{max} (°C)
q
θ
$\Delta T_{surface}$
T_{max}
T_o = 2000 °C
$\langle q \rangle$ = 150 W/cm^2
L = 1.5 cm
REP. RATE = 20 S^{-1}
10^{-7}
10^{-5}
10^{-3}
5×10^{-2}
PULSE WIDTH (sec)

FIGURE 5

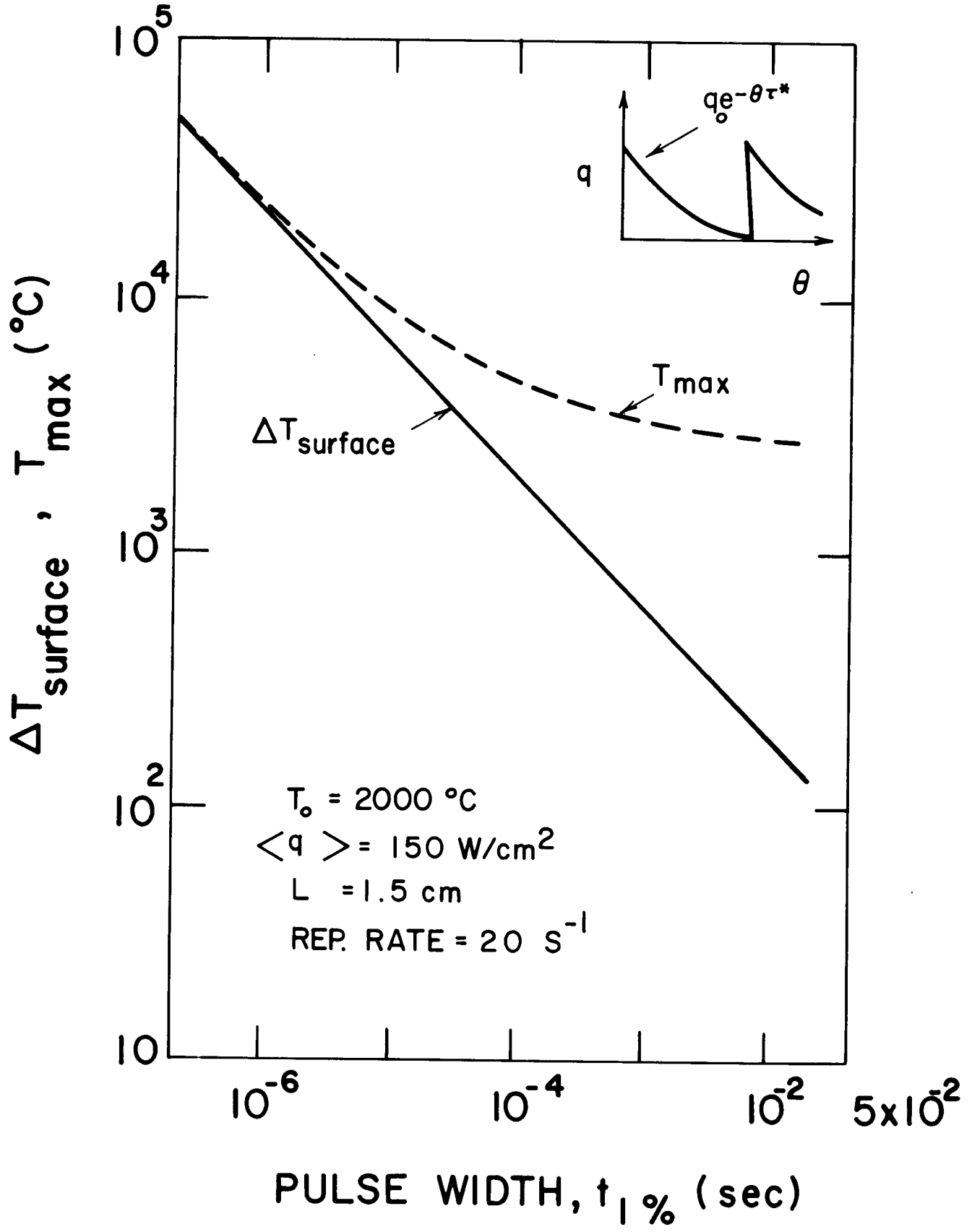
10^5
10^4
10^3
10^2
10
$\Delta T_{surface}$, T_{max} (°C)
$qe^{-\theta\tau^*}$
q
θ
T_{max}
$\Delta T_{surface}$
T_o = 2000 °C
$\langle q \rangle$ = 150 W/cm^2
L = 1.5 cm
REP. RATE = 20 s^{-1}
10^{-6}
10^{-4}
10^{-2}
$5x10^{-2}$
PULSE WIDTH, $t_{1\%}$ (sec)

FIGURE 6

LIGHT ION BEAM REACTOR CAVITY AND FIRST WALL

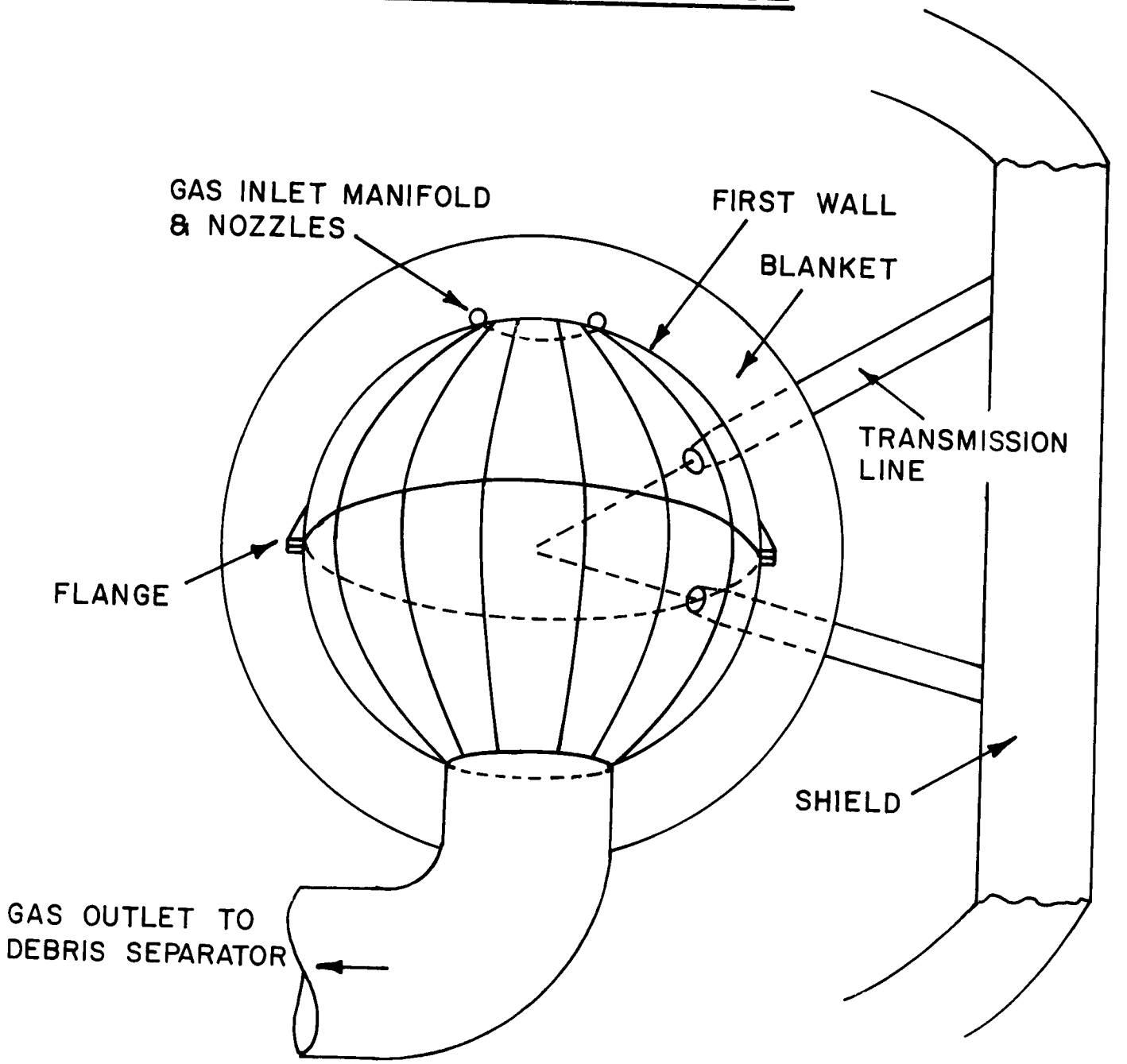

FIGURE 7

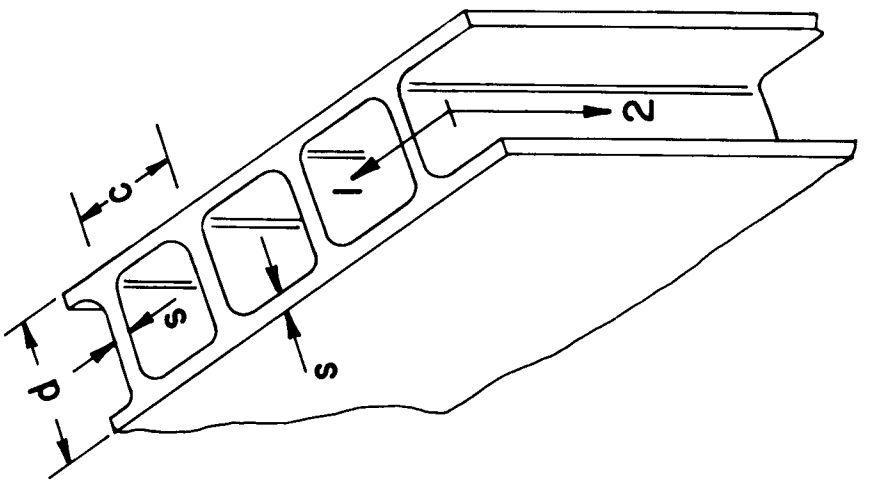

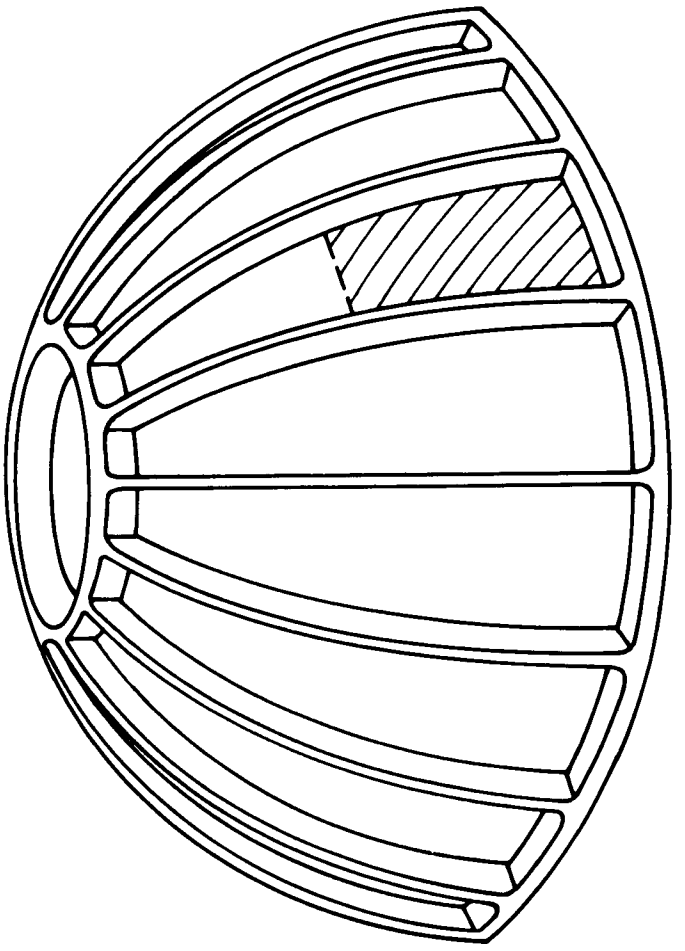

FIGURE 8

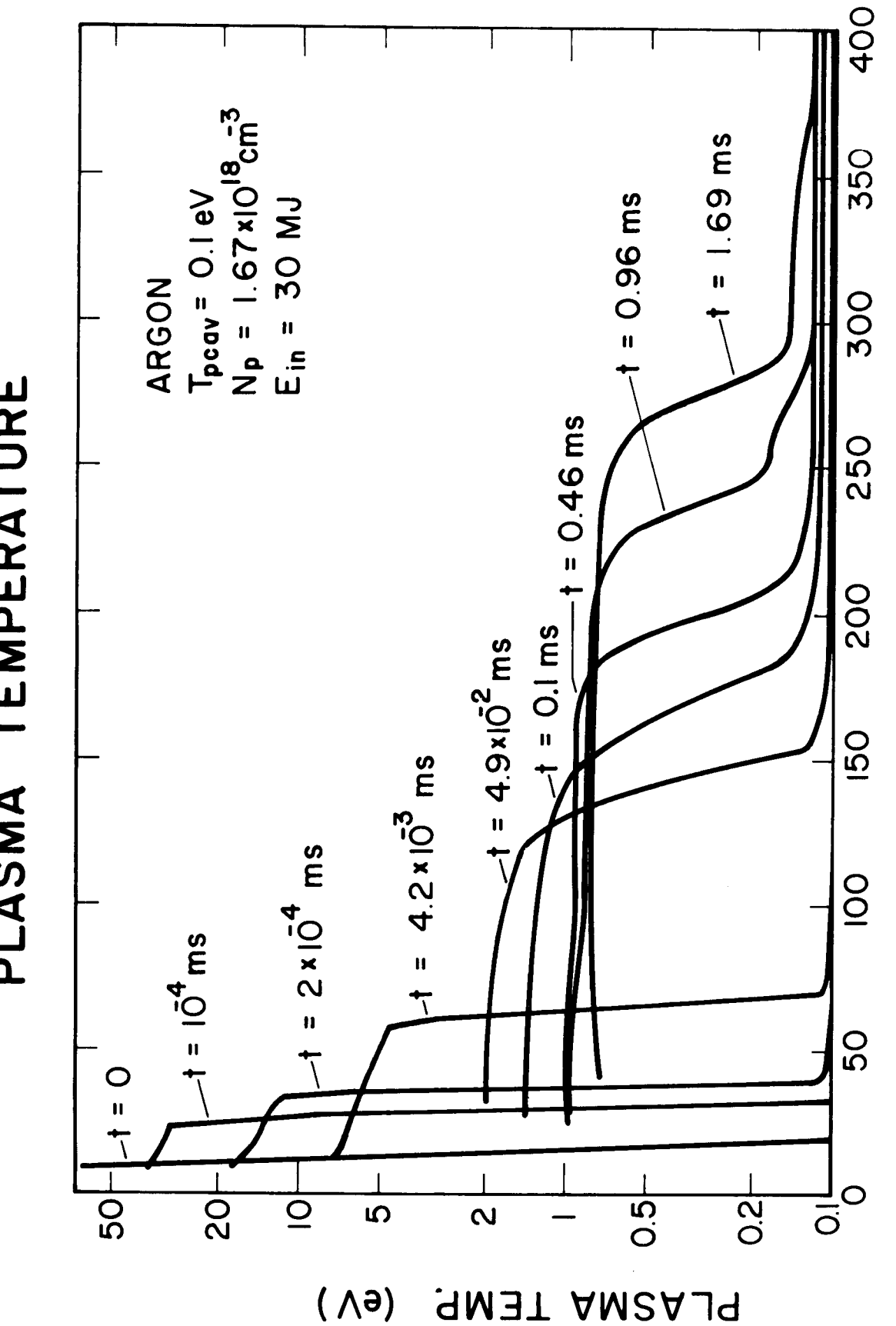
PLASMA TEMPERATURE
ARGON
T_{pcav} = 0.1 eV
N_p = 1.67x10^{18}cm^{-3}
E_{in} = 30 MJ
t = 0
t = 10^{-4} ms
t = 2x10^{-4} ms
t = 4.2x10^{-3} ms
t = 4.9x10^{-2} ms
t = 0.1 ms
t = 0.46 ms
t = 0.96 ms
t = 1.69 ms
PLASMA TEMP. (eV)
50
20
10
5
2
1
0.5
0.2
0.1
0
50
100
150
200
250
300
350
400
RADIUS (cm)

FIGURE 9

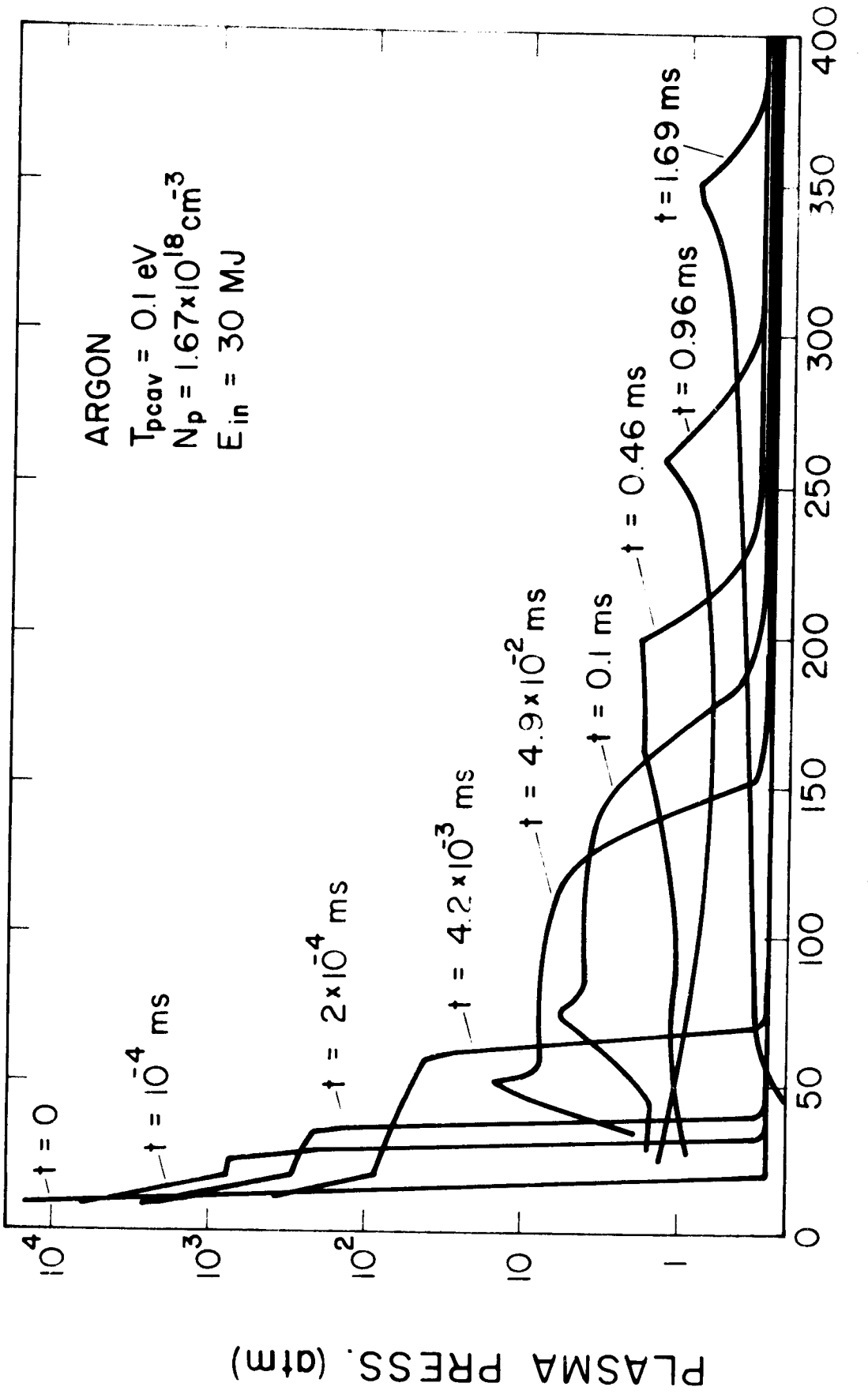
PLASMA PRESSURE
ARGON
T_{pcav} = 0.1 eV
$N_p = 1.67 \times 10^{18} cm^{-3}$
E_{in} = 30 MJ
t = 0
$t = 10^{-4}$ ms
$t = 2 \times 10^{-4}$ ms
$t = 4.2 \times 10^{-3}$ ms
$t = 4.9 \times 10^{-2}$ ms
t = 0.1 ms
t = 0.46 ms
t = 0.96 ms
t = 1.69 ms
PLASMA PRESS. (atm)
10^4
10^3
10^2
10
1
0
50
100
150
200
250
300
350
400
RADIUS (cm)

FIGURE 10

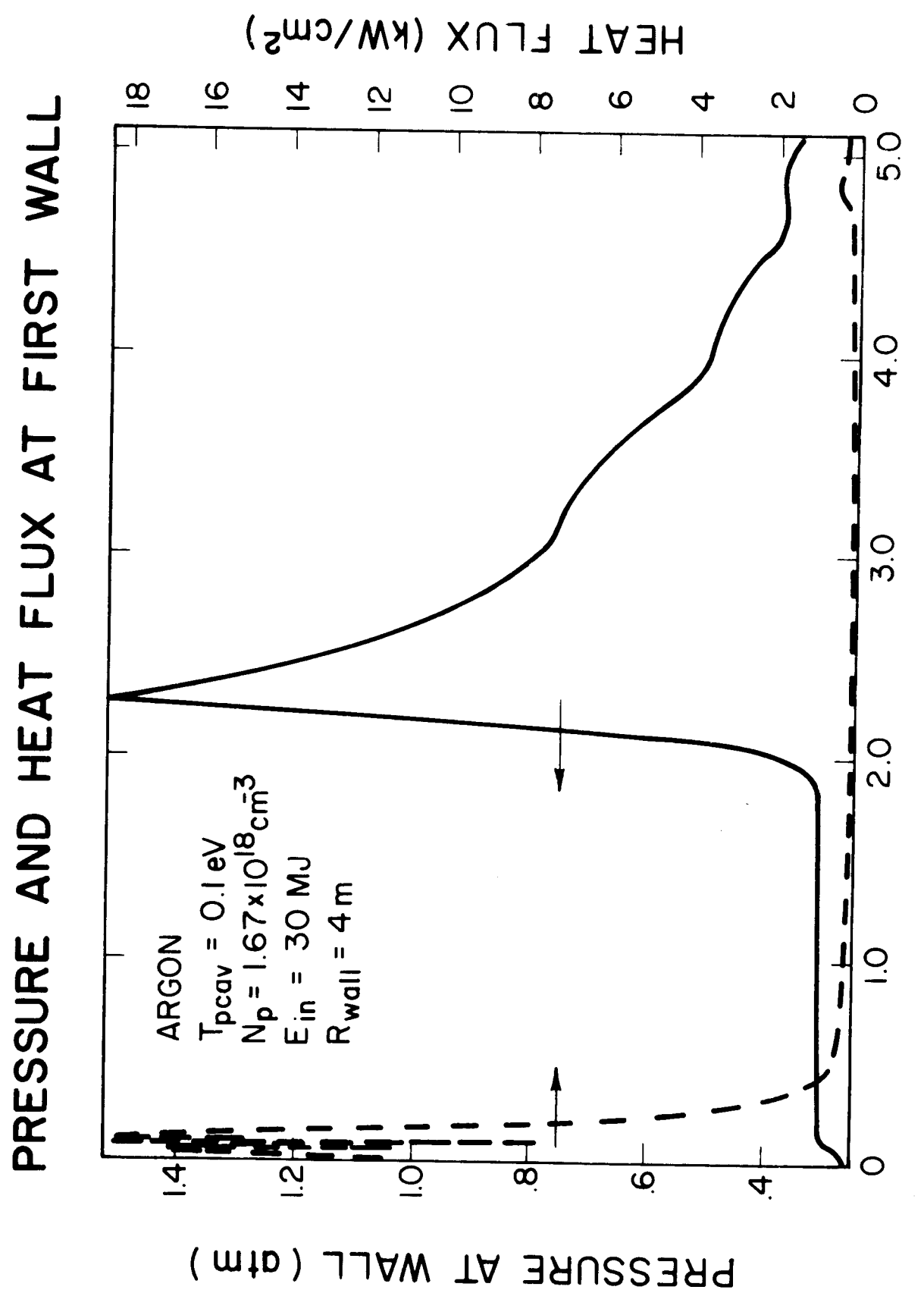
PRESSURE AND HEAT FLUX AT FIRST WALL
ARGON
T_{pcav} = 0.1 eV
N_p = 1.67x10^{18}cm^{-3}
E_{in} = 30 MJ
R_{wall} = 4m
PRESSURE AT WALL (atm)
HEAT FLUX (kW/cm^2)
TIME (msec)
1.4
1.2
1.0
.8
.6
.4
18
16
14
12
10
8
6
4
2
0
0
1.0
2.0
3.0
4.0
5.0

FIGURE 11

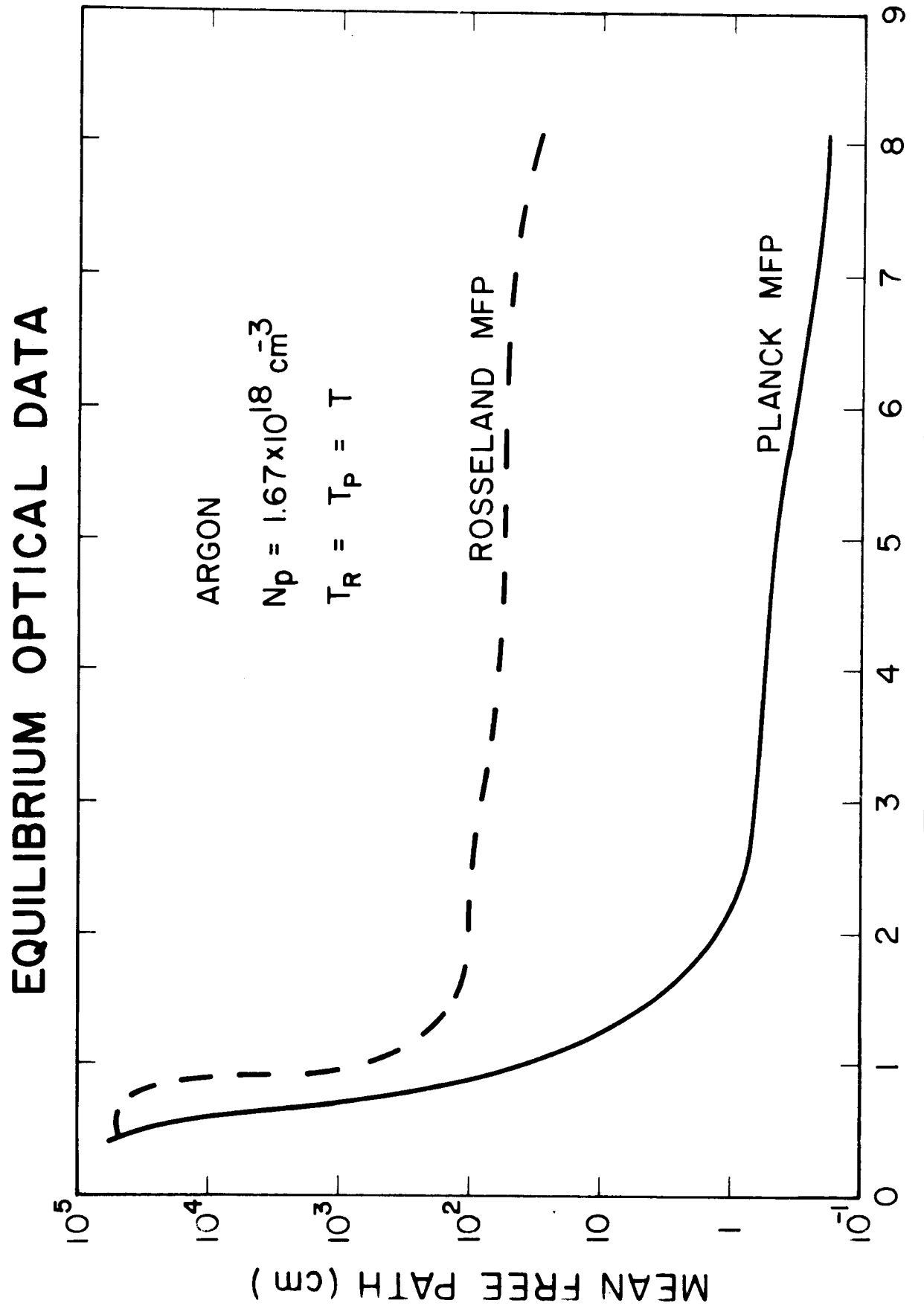
EQUILIBRIUM OPTICAL DATA
ARGON
$N_p = 1.67 \times 10^{18}\ cm^{-3}$
$T_R = T_P = T$
ROSSELAND MFP
PLANCK MFP
MEAN FREE PATH (cm)
10^5
10^4
10^3
10^2
10
1
10^{-1}
0
1
2
3
4
5
6
7
8
9
TEMPERATURE T (eV)

FIGURE 12

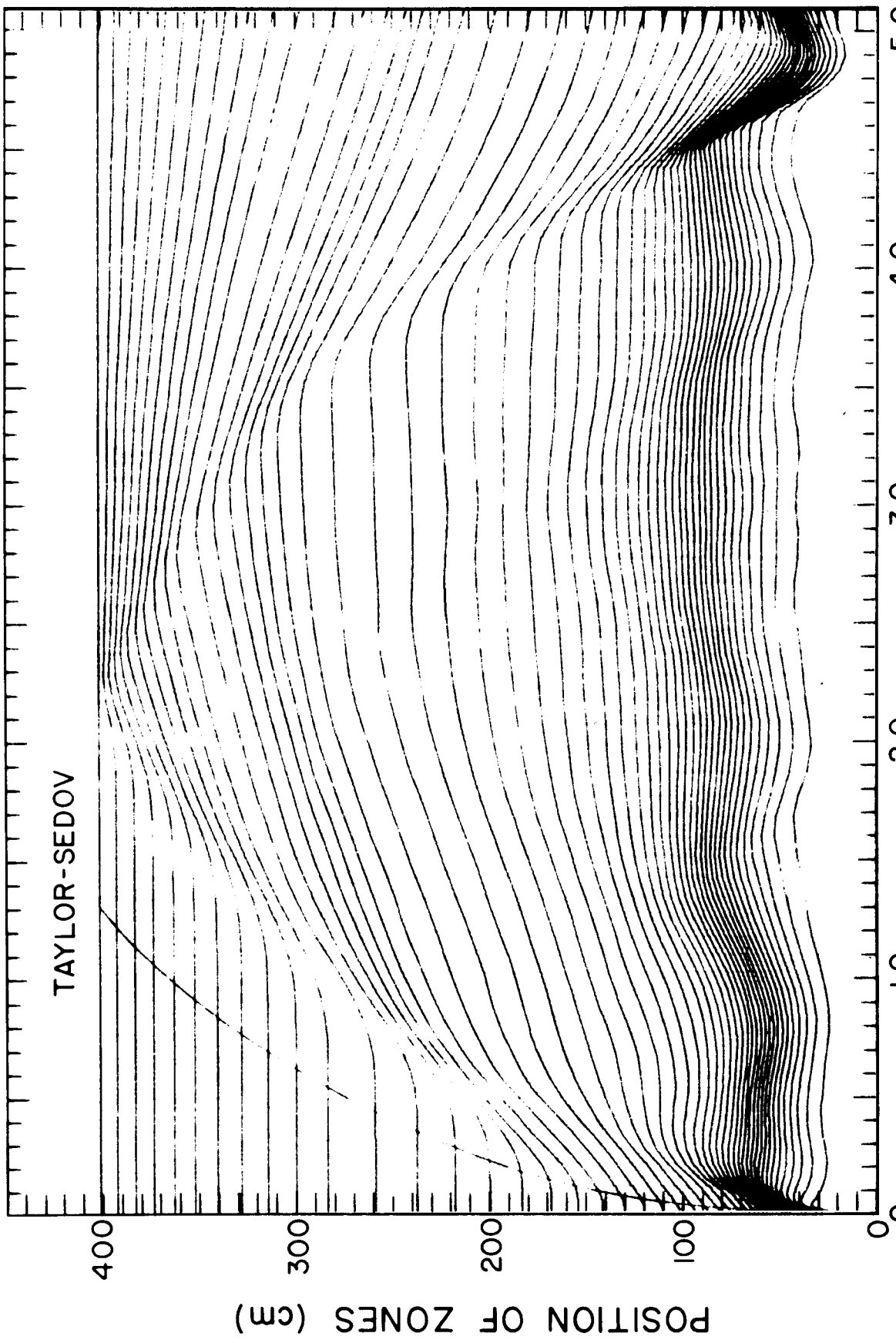
SHOCK PROPAGATION IN ARGON
T_{pcav} = 0.1 eV , N_p = 1.67x10^{18}cm^{-3} , E_{in} = 30 MJ
TAYLOR-SEDOV
POSITION OF ZONES (cm)
400
300
200
100
0
0
1.0
2.0
3.0
4.0
5.0
TIME (msec)

FIGURE 13

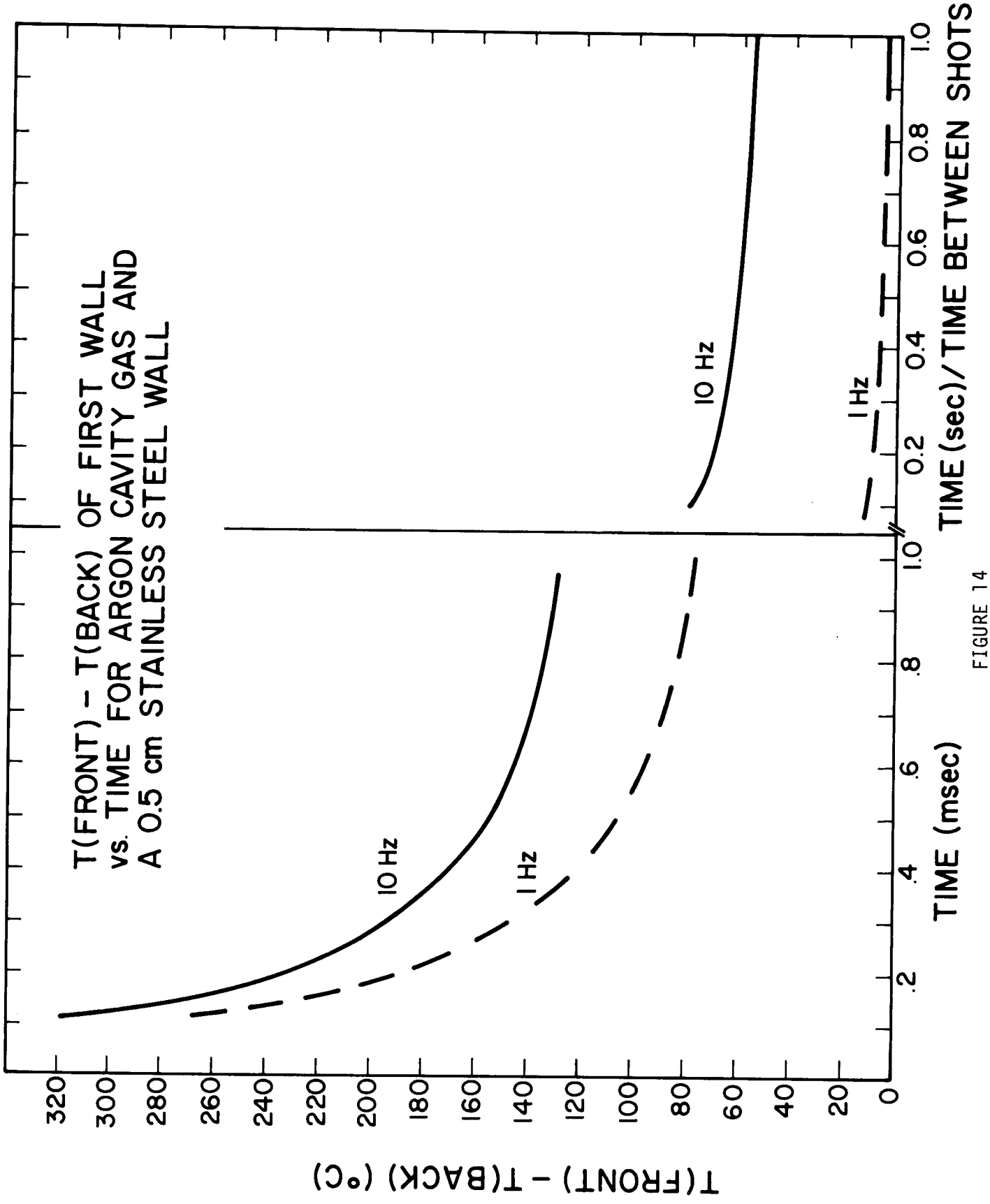
T(FRONT) - T(BACK) OF FIRST WALL
vs. TIME FOR ARGON CAVITY GAS AND
A 0.5 cm STAINLESS STEEL WALL
10 Hz
1 Hz
10 Hz
1 Hz
T(FRONT) - T(BACK) (°C)
TIME (msec)
TIME (sec)/TIME BETWEEN SHOTS
0
20
40
60
80
100
120
140
160
180
200
220
240
260
280
300
320
.2
.4
.6
.8
1.0
0.2
0.4
0.6
0.8
1.0

FIGURE 14

PRESSURE AND HEAT FLUX AT FIRST WALL

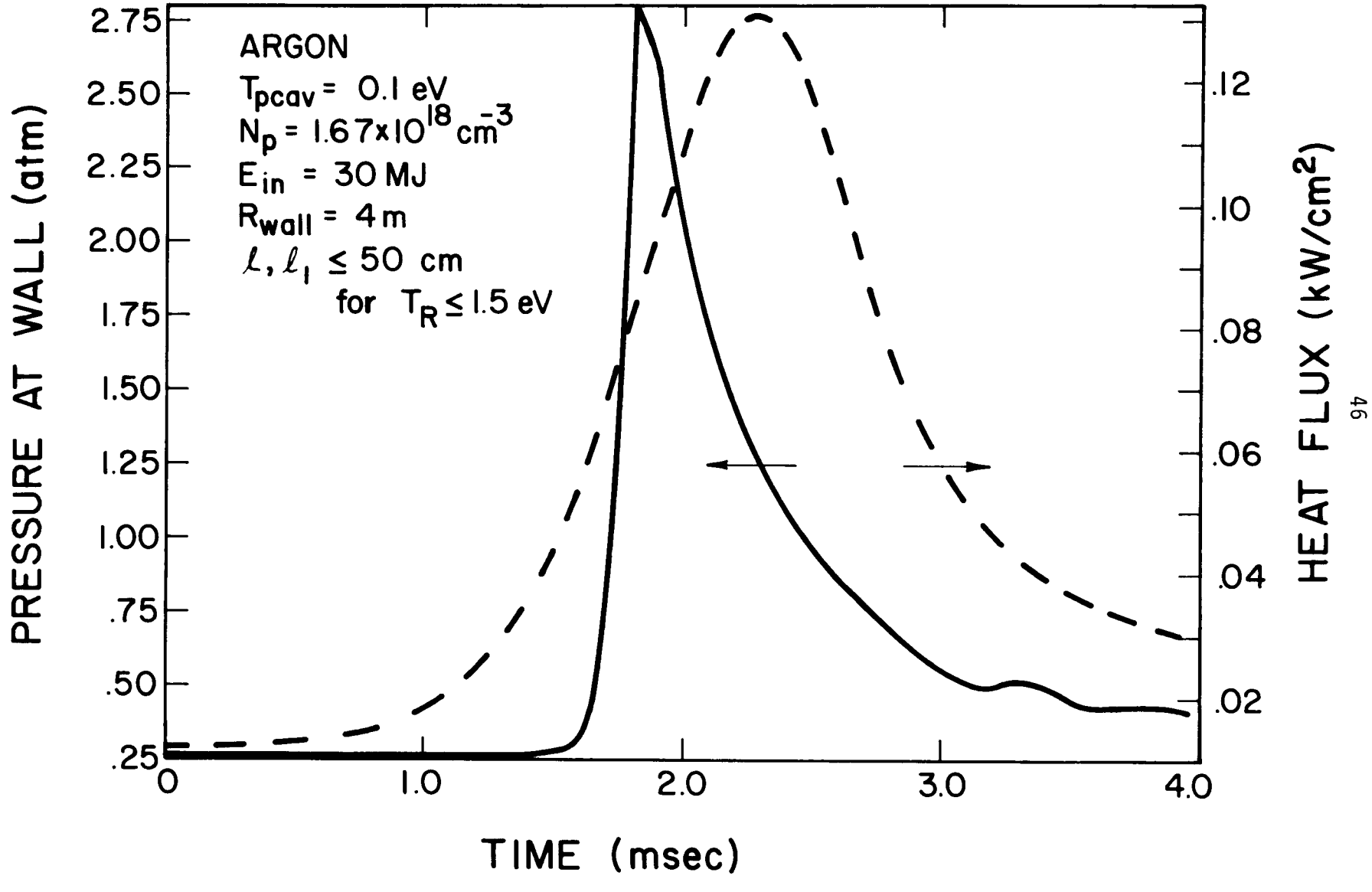

FIGURE 15